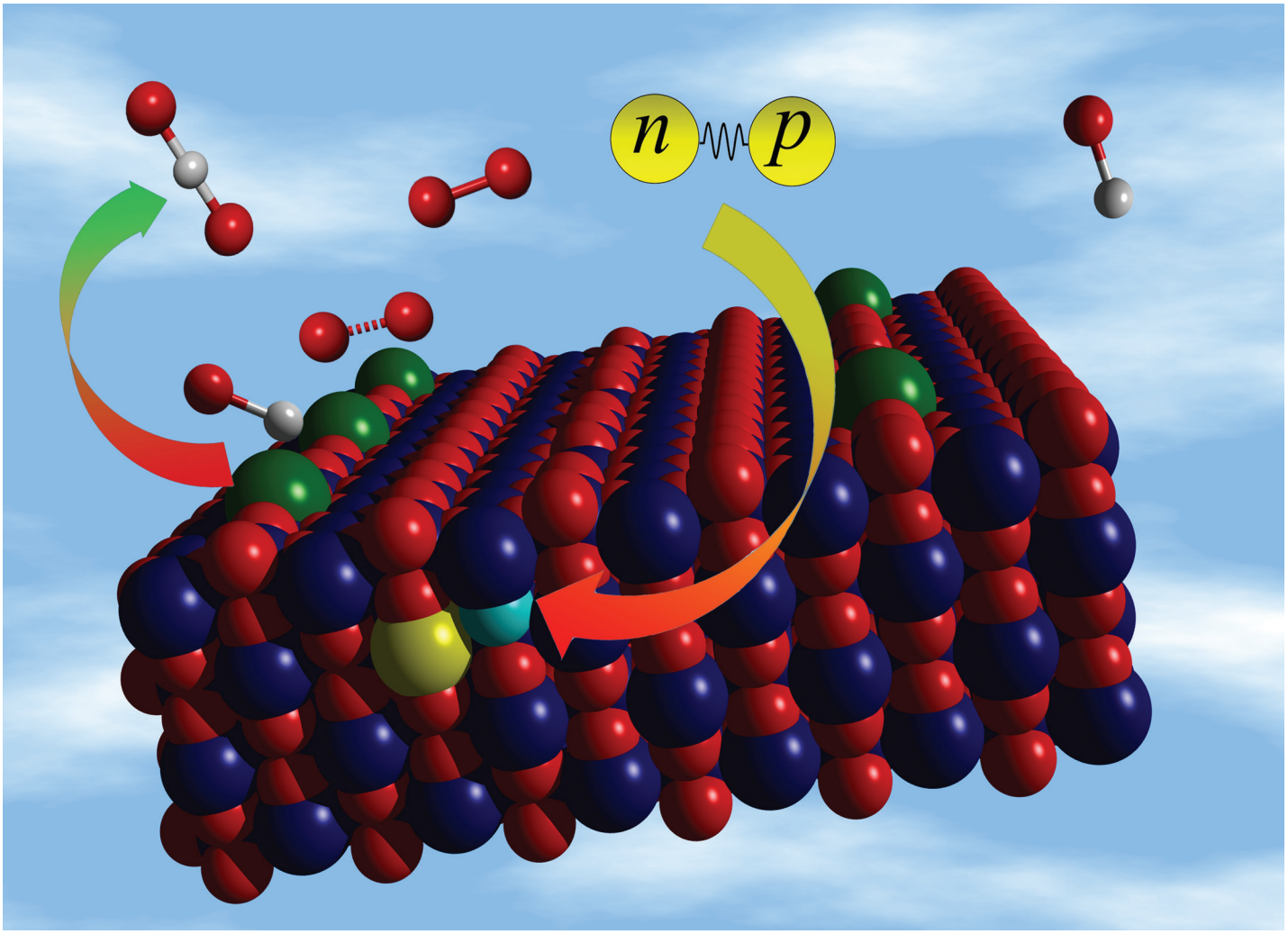

Showcasing research from Prof. Shunfang Li at the International Laboratory for Quantum Functional Materials of Henan, Zhengzhou University, China, in collaboration with Prof. Z. X. Guo, at University College London.

Substrate co-doping modulates electronic metal–support interactions and significantly enhances single-atom catalysis

Theory predicts the key steps in CO oxidation by a Pd single atom catalyst (SAC) deposited on a pristine rutile TiO_2(110) substrate and those with embedded metal-nonmetal n-p co-dopant pairs, to elucidate the role of electronic metal-support interactions (EMSIs) in tuning the catalysis of SACs. We show that the EMSIs can provide a crucial degree of freedom to enhance the catalysis of an, otherwise, inert Pd SAC for O_2 activation and CO oxidation.

As featured in:

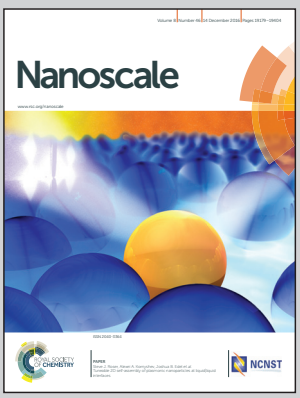

See Z. X. Guo, S. F. Li *et al.*, *Nanoscale*, 2016, **8**, 19256.

ROYAL SOCIETY OF CHEMISTRY

www.rsc.org/nanoscale

Registered charity number: 207890

Nanoscale

PAPER

View Article Online
View Journal | View Issue

Cite this: *Nanoscale*, 2016, **8**, 19256

Substrate co-doping modulates electronic metal–support interactions and significantly enhances single-atom catalysis†

J. L. Shi,[a] J. H. Wu,[b] X. J. Zhao,[a] X. L. Xue,[a] Y. F. Gao,[c,d] Z. X. Guo*[e,a] and S. F. Li*[a]

Transitional metal nanoparticles or atoms deposited on appropriate substrates can lead to highly economical, efficient, and selective catalysis. One of the greatest challenges is to control the electronic metal–support interactions (EMSI) between the supported metal atoms and the substrate so as to optimize their catalytic performance. Here, from first-principles calculations, we show that an otherwise inactive Pd single adatom on TiO_2(110) can be tuned into a highly effective catalyst, *e.g.* for O_2 adsorption and CO oxidation, by purposefully selected metal–nonmetal co-dopant pairs in the substrate. Such an effect is proved here to result unambiguously from a significantly enhanced EMSI. A nearly linear correlation is noted between the strength of the EMSI and the activation of the adsorbed O_2 molecule, as well as the energy barrier for CO oxidation. Particularly, the enhanced EMSI shifts the frontier orbital of the deposited Pd atom upward and largely enhances the hybridization and charge transfer between the O_2 molecule and the Pd atom. Upon co-doping, the activation barrier for CO oxidation on the Pd monomer is also reduced to a level comparable to that on the Pd dimer which was experimentally reported to be highly efficient for CO oxidation. The present findings provide new insights into the understanding of the EMSI in heterogeneous catalysis and can open new avenues to design and fabricate cost-effective single-atom-sized and/or nanometer-sized catalysts.

Received 27th May 2016,
Accepted 6th October 2016

DOI: 10.1039/c6nr04292a

www.rsc.org/nanoscale

Introduction

Transitional metal (TM) and noble metal (NM) nanoparticles supported on oxide surfaces have been extensively used as efficient and economical catalysts in many industrial applications, such as CO oxidation in vehicle emission reduction,[1–3] water–gas shift reaction,[4] and hydrogenation.[5] However, the intrinsic catalytic activities and selectivity of these supported metal particles are strongly size- and geometry-dependent, particularly at the nanometer and sub-nanometer scales. In such regimes, the catalysis of TMs/NMs even with a given shape is characterized by a significant size effect, due to the variation of the increasingly large fraction of the low-coordinate metal atoms that often function as active sites for catalysis.[6–8] As the ultimate size limit, single-atom catalysts (SACs) deposited uniformly on appropriate substrates are widely expected to maximize the efficiency, activity and selectivity of TM and NM catalysts, particularly for the latter. For example, SACs of Pt, Rh, Pd and Ru on FeO_x are reported to exhibit high performance for O_2 activation and CO oxidation.[9] A single Fe atom embedded in a silica matrix enhances methane activation.[10] However, it was also experimentally reported that the catalytic activity for CO oxidation is insignificant for single Pd atoms on TiO_2(110), but is substantially higher for Pd ad-dimers and larger adsorbed clusters.[3] Similarly, Au monomers show negligible catalytic activity on TiO_2(110) for CO oxidation though Au single atoms exhibit excellent catalysis on other substrates.[4,11]

Clearly, the substrate also plays a crucial role in the chemical activity and selectivity of the deposited nanocatalysts,[12–14] as first recognized by Tauster *et al.*[13] in 1978, and now well known as the "strong metal–support interactions (SMSI)". Recently, Bruix *et al.*[14] provided an in-depth analysis of the effect of SMSI on the significantly enhanced activity of Pt particles on ceria in water–gas shift reactions. More specifically, Campbell[15] coins the findings of Bruix and co-workers[14] as "electronic metal–support interactions" (EMSI) manifested by

[a]*International Laboratory for Quantum Functional Materials of Henan, School of Physics and Engineering, Zhengzhou University, Zhengzhou, Henan 450001, China. E-mail: sflizzu@zzu.edu.cn*
[b]*Department of Physics, Henan Institute of Education, Zhengzhou, 450046, China*
[c]*Department of Materials Science and Engineering, University of Tennessee, Knoxville, Tennessee 37996, USA*
[d]*Materials Science and Technology Division, Oak Ridge National Laboratory, Oak Ridge, Tennessee 37831, USA*
[e]*Department of Chemistry, University College London, London WC1H 0AJ, UK*

†Electronic supplementary information (ESI) available: Details on the simulation methods, additional data are presented in Fig. S1–S5. See DOI: 10.1039/c6nr04292a

the chemical bonding and associated charge transfer at the metal–support interface. Namely, the enhanced activity of the deposited particles may be essentially attributed to electronic perturbations that modify the electronic states of the deposited metal and improve their catalytic properties due to the EMSI. To demonstrate more convincingly the importance of the EMSI in the activity of a metal catalyst, it is imperative to focus on SAC systems,[16] which can unambiguously rule out other factors, such as the electronic quantum size effect[17,18] and structural sensitivity[19,20] involved in nanoparticles. In Hu and co-worker's recent experiment the role of the EMSI is established by comparison of the activities of Ag-SACs on two types of supports but with different local geometric structures, which in some sense dilutes the pure electronic effect of the EMSI.

Here, using the state-of-the-art first-principles calculations, we consider a Pd atom supported in the vicinity of the surface oxygen vacancy of the rutile TiO_2(110), Pd@TiO_2(110), as a representative SAC for CO oxidation, to establish the role of a pure electronic effect in the EMSI in controlling the catalysis of a given SAC. A comparative investigation was carried out for the catalysis of Pd@TiO_2(110) and those with metal–nonmetal co-dopant pairs in the sub-layer, while keeping the local geometric structure of the Pd atom almost constant. In contrast to Bruix's model catalyst, the present systems can mostly rule out the geometric effect of the substrates in identifying the "pure" electronic contribution to the EMSI effect. Intriguingly, a nearly linear correlation between the strength of the EMSI and the CO oxidation rate was established in the studied systems, *i.e.*, the stronger the EMSI, the larger the CO oxidation rate.

Methods

Our DFT calculations[21] were performed using the Vienna *ab initio* simulation package (VASP)[22] with the projector augmented wave (PAW)[23] method. For the exchange–correlation energy, we employed the generalized gradient approximation functional of Perdew–Burke–Ernzerhof.[24] Simulation details are presented in S1 of the ESI.†

Results and discussion

First of all, we confirm that the Pd single atom prefers to be located in the vicinity of the surface oxygen vacancy (V_O) site of the TiO_2(110) surface, as deduced from both the energetics and low diffusion rates of the Pd atoms observed in the experiment,[25] supported also by recent state-of-the-art first-principles calculations.[26] Based on this, the O_2 adsorption and CO oxidation process are re-examined by extensive additional calculations. The present results are in close agreement with previous calculations,[26] *i.e.*, the O_2 molecule can only weakly adsorb on the Pd@TiO_2(110) complex with an adsorption energy, *i.e.*, $E_{ads}(O_2)$ = 0.241 eV, and the CO oxidation experiences a large activation barrier of 1.132 eV. Therefore, both the small binding energy and the large CO oxidation barrier together determine the low catalytic activity of Pd@TiO_2(110). For more details on the geometric structure of Pd@TiO_2(110) and the minimum energy path for CO oxidation on it, see Fig. S1.†

To optimize the chemical activity of the intrinsically inert Pd@TiO_2(110), co-doping is invoked here to modulate the electronic structures of the TiO_2(110) substrate and consequently tune the EMSI between the Pd metal atom and the co-doped substrates. It is widely accepted that the substitutional doping of a binary oxide semiconductor is extremely difficult due to the limited solubility of the dopants, especially for p-type doping.[27] Recently, Zhu *et al.*[28] reported that the introduction of donor–acceptor co-dopant pairs is an effective approach to enhance the solubility of dopants in TiO_2. In view of this, we choose two typical 3d transition metals, V and Cr, as the n-type dopants to substitute for a Ti atom, and two nonmetal elements, N and C, as the p-type dopants to substitute for a neighboring O site, respectively. Therefore, four metal–nonmetal co-dopant pairs can be obtained, *i.e.*, p-type V–C, compensated V–N and Cr–C, and n-type Cr–N, respectively.

Fig. 1 depicts the most stable configurations of the four co-doped Pd@TiO_2(110) complexes. Energetically, it is confirmed that the co-dopant pairs do prefer to form a metal–nonmetal dimer in Pd@TiO_2(110), due to the strong Columbic electrostatic attraction between the metal donor and nonmetal acceptor ions. Consequently, the introduction of co-dopant pairs into the TiO_2 substrate leads to three important features for the binding of the Pd on the defective TiO_2(110) surface. Firstly, without co-doping, the Pd atom favors exactly the V_O site, whereas it slightly departs from the V_O in the co-doped cases; however, upon O_2 and CO co-adsorption, the Pd atom on pristine TiO_2(110) also relaxes to the same local site as that in the co-doped cases, which will be discussed later. Secondly, as shown in Fig. 1, the Pd atom possesses similar local supporting structures in all the four co-doped cases. For details on the bond lengths of the Pd atom with the substrates, see S3 of the ESI.† Thirdly, the co-dopant pairs enhance the electronic binding of the Pd atom with the TiO_2(110) substrate, *i.e.*, from 1.641 to 1.788, 1.769, 1.768 and 1.768 eV, for the un-doped, V–C, V–N, Cr–C, and Cr–N co-doped Pd@TiO_2(110), respectively.

Now, we discuss the doping effect in modulating the electronic structures of the Pd atom through the EMSI. In Fig. 2,

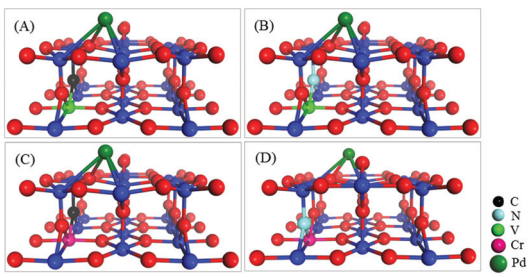

Fig. 1 Local geometric structures of co-doped Pd@TiO_2(110) complexes with (A) V–C; (B) V–N; (C) Cr–C; and (D) Cr–N co-dopant pairs.

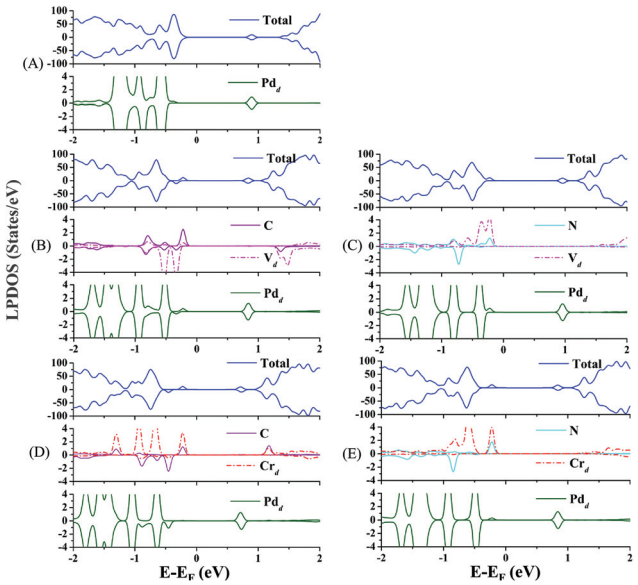

Fig. 2 Total and local projected density of states (DOS) of (A) pristine rutile Pd@TiO_2(110); and that of (B) V–C, (C) V–N, (D) Cr–C and (E) Cr–N co-doped systems.

the total density of states (DOS) of the co-doped Pd@TiO_2(110) species including the local projected DOS (LPDOS) of the dopants and the Pd atom are presented. For comparison, the LPDOS of the un-doped Pd@TiO_2(110) are also shown in Fig. 2(A). As shown in Fig. 2(B)–(E), the energy gap between the valence band maximum (VBM) and the conduction band minimum (CBM) is significantly reduced by co-doping. Specifically, in the un-doped Pd@TiO_2(110) system, the VBM is dominated by the p orbital of the O atoms and the CBM is located in the vicinity of the lowest-unoccupied-molecular-orbital (LUMO) of the Pd atom, respectively. In addition, the HOMO–LUMO gap (E_{gap}(HOMO–LUMO)) of the Pd atom is about 1.464 eV. Upon doping, both the VBM and CBM are changed due to the introduction of the co-dopant states and the resulting EMSI. Distinctly, in all these four co-doped cases, the VBM is shifted upward and now positioned in the vicinity of the HOMO of the co-dopant pairs (see Fig. 2(B)–(E)), and the CBM is further lowered except for the cases of V–N co-doping (see Fig. 2(C)). Importantly, the frontier orbital (HOMOs) of the Pd atom hybridizes with the co-dopant states by the Fermi level, which effectively shifts the HOMOs of the Pd single atom upwards. For example, in the p-type V–C co-doped complex, the (d-electron dominated) HOMOs of the P atom hybridize with the HOMOs of the V atom and those of the C atom in the energy window of −0.6 to −0.3 eV. Furthermore, the HOMO of the Pd atom is now upward shifted by about 0.5 eV, see Fig. 2(B). Moreover, such an orbital hybridization between the Pd atom and the substrate, particularly with the doped metal cations, is accompanied by charge transfer from the former to the latter *via* a charge compensation mechanism. Therefore, such a charge transfer leads the Pd atom to depart from its closed-shell (d^{10}) characteristics, and is now positively charged, as confirmed by the Bader charge analysis presented in Table 1. Here, we emphasize that it is just the hybridization and charge transfer that increase the HOMO of the Pd atom and enhance its chemical activity towards oxygen adsorption and activation, which will be illustrated shortly.

Adsorption of O_2 molecules on co-doped Pd@TiO_2(110) SACs

To further identify the co-doping effect in modulating the chemical activity of the Pd atom *via* the EMSI, we now investigate the key process of CO oxidation, *i.e.*, the adsorption and activation of an O_2 molecule on the co-doped structures presented in Fig. 1. Upon extensive calculations, we identified the most stable configurations for O_2 adsorption on the four co-doped Pd@TiO_2(110) complexes, as shown in Fig. 3. Note that in the optimized O_2-Pd@TiO_2(110) co-doped structures, the

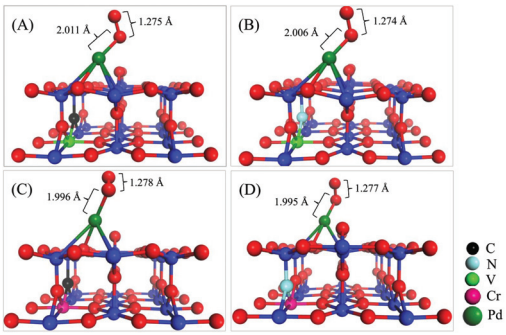

Fig. 3 Geometric O_2 adsorption structures of co-doped Pd@TiO_2(110) complexes with (A) V–C; (B) V–N; (C) Cr–C; and (D) Cr–N co-dopant pairs.

Table 1 Effect of co-doping on the O_2 activation by Pd@TiO_2(110). Calculated binding energy, E_b(Pd) and charge state Q(Pd) of the Pd single atom on pristine and co-doped rutile Pd@TiO_2(110) surfaces. The adsorption energy, E_{ads}(O_2); O–O bond length, R(O–O); charge transfer, Q(O_2) and the stretching vibrational frequency, ω of the lowest energy structures of an O_2 molecule adsorption on pristine and co-doped rutile Pd@TiO_2(110) surfaces

Systems	E_b(Pd)(eV)	Q(Pd)(e)	E_{ads}(O_2)(eV)	R(O–O)(Å)	Q(O_2)(e)	ω(cm^{-1})
Pd@TiO_2(110):V–C	1.788	+0.161	0.808	1.275	0.22	1296.32
Pd@TiO_2(110):V–N	1.769	+0.160	0.732	1.274	0.21	1302.04
Pd@TiO_2(110):Cr–C	1.768	+0.164	0.794	1.278	0.22	1284.58
Pd@TiO_2(110):Cr–N	1.768	+0.162	0.801	1.277	0.23	1348.51
Pd@TiO_2(110)	1.641	+0.158	0.241	1.254	0.10	1560.83

Pd atoms only binds directly with one oxygen atom of the O_2 molecule, which is very similar to the O_2 adsorption on other low dimensional noble metal structures.[29,30] In contrast to the case of the un-doped Pd@TiO_2(110), the O_2 molecule is found to bind strongly to the Pd atom deposited on the doped TiO_2(110) substrates. Specifically, as summarized in Table 1, the adsorption energy ($E_{ads}(O_2)$) of the O_2 molecule is increased from 0.241 to 0.808, 0.732, 0.794, and 0.801 eV, for pristine Pd@TiO_2(110), the V–C, V–N, Cr–C, and Cr–N co-doped complexes, respectively. Meanwhile, in the V–C, V–N, Cr–C, and Cr–N co-doped cases, the stretching vibrational frequency of the adsorbed O_2 molecule is further red-shifted from 1560.83 to 1296.32, 1302.04, 1284.58, and 1348.51 cm^{-1}, due to the enlarged O–O bond lengths, *i.e.*, 1.275, 1.274, 1.278, and 1.277 Å, respectively. These data convincingly indicate that the O_2 molecule is considerably activated on these co-doped Pd@TiO_2(110) SACs due to the enhanced EMSI.

Now, we further explore the underlying mechanism of the EMSI in improving the chemical activity of the Pd atom *via* co-doping. In doing so, we analyze the DOS of the optimized final states of the O_2 molecule adsorbed on the Pd atom on TiO_2(110) co-doped by V–C, V–N, Cr–C, and Cr–N pairs, respectively. In Fig. 4(B)–(E), the LPDOS of all the Ti atoms, Pd atoms, co-dopant pairs, and the adsorbed O_2 species are presented. In addition, the DOS for O_2 on the un-doped Pd@TiO_2(110) is also shown as a comparison in Fig. 4(A). Here, to illustrate more clearly the role of the EMSI, we only focus on an energy window of −2.0 to 2.0 eV by the Fermi level in analyzing the DOS. As shown in Fig. 4(A), for O_2 adsorption on the un-doped Pd@TiO_2(110), there is negligible hybridization between the HOMO of the deposited Pd atom and the LUMO of the O_2 molecule, due to the relatively deep energy level of the HOMO and the large E_{gap}(HOMO(Pd)–LUMO(O_2)). Therefore, O_2 can only weakly bind to the Pd@TiO_2(110) SAC with a minor charge transfer obtained by Bader charge analysis, *i.e.*, about 0.1*e* from the Pd to the adsorbed O_2 species. However, upon co-doping, the d-electron dominated HOMO of the Pd atom hybridizes with that of the co-dopant pairs in the vicinity of the Fermi level. These hybridized filled states serve as an effective electron reservoir for the incoming O_2 molecule to capture the electron charge. More specifically, taking the O_2 adsorption on the Cr–N co-doped case as an example, one can see that though the Pd atom only slightly hybridizes with the HOMO (which is about 0.2 eV below the Fermi level) of the Cr atom, in the final state, such an orbital hybridization is significantly enhanced, see Fig. 4(E); meanwhile, for the adsorbed O_2 molecule there exists considerable spin-minority LPDOS hybridization with that of the Pd atom around 0.7 eV below the Fermi level. We emphasize that when the O_2 molecule is far away from the Pd atom, the spin-minority LPDOS (O_2) is about 1.2 eV above the Fermi level and totally unfilled. These results confirm an evident charge transfer (about 0.3*e*) from the SAC to the O_2 molecule. Therefore, one can conclude that the n-type Cr–N pair (essentially the metal Cr) plays an important role in serving as the charge reservoir, compensating for the charge of the Pd atom, and thus enhancing the interaction with the O_2 molecule. Subsequently, such a charge transfer weakens the O–O bond and further strengthens the O_2 activation as manifested by the enlarged $E_{ads}(O_2)$ of 0.801 eV and red-shifted stretching vibration frequency of 1348.51 cm^{-1}, see Table 1.

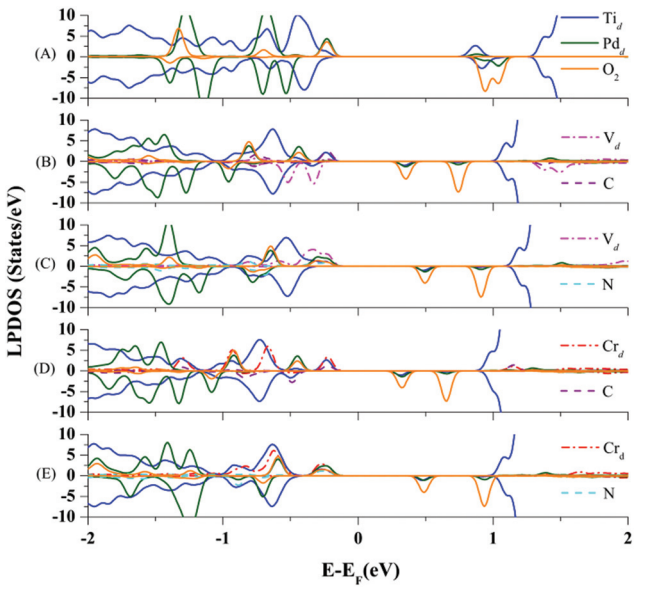

Fig. 4 Local projected density of states of optimized structures for O_2 molecule adsorption on (A) pristine rutile Pd@TiO_2(110); and that of (B) V–C, (C) V–N, (D) Cr–C and (E) Cr–N co-doped complexes.

Note that the p-type V–C, and the two compensated V–N and Cr–C couplings also significantly facilitate the O_2 adsorption and activation *via* a similar mechanism due to the enhanced EMSI. As shown in Fig. 3(B)–(D), the co-dopant-assisted enhanced hybridizations between the Pd atom and the O_2 molecule are also observed in the energy range of −1.0 to 1.0 eV by the Fermi levels. Such interactions stimulate the charge transfer between the O_2 molecule and SAC, and enhance the O_2 activation, as seen from the calculated data summarized in Table 1. Based on the present findings, we can conclude that the chemical activity of the intrinsically inert Pd atom can be effectively optimized by the EMSI *via* the co-doping approach. To further identify the dominated intrinsic parameter in such an optimization rule, we analyze the DOS of the O_2 molecule far (about 5.0 Å) above these co-doped Pd@TiO_2(110) SACs, including other n-type co-doping, such as the Cr–S pair; for details, see S4 of the ESI.† We find that, overall, the smaller the E_{gap}(HOMO(Pd)–LUMO(O_2)), the larger the $E_{ads}(O_2)$, as presented in Fig. 5, in line with the well-known d-band theory.[31,32] Note again that, as presented in the ESI (S4)† and the above discussion, the reduced E_{gap}(HOMO(Pd)–LUMO(O_2)) originates from an enhanced EMSI through n–p co-doping, *i.e.*, the stronger the EMSI, the smaller the E_{gap}(HOMO(Pd)–LUMO(O_2)); and consequently the stronger the O_2 activation.

CO oxidation on n–p co-doped Pd@TiO_2(110)

Having clearly illustrated the critical step of O_2 activation on the n–p co-doped Pd@TiO_2(110) systems, we continue to inves-

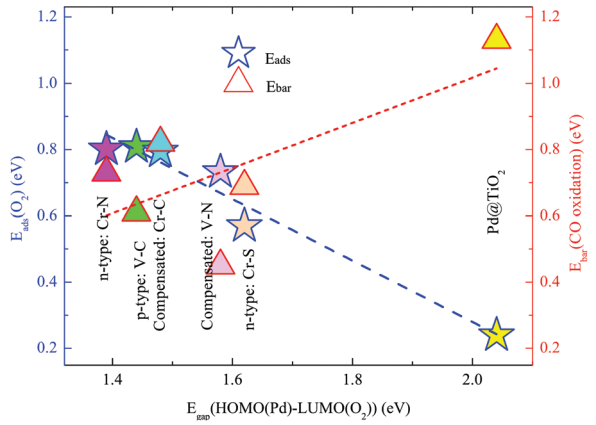

Fig. 5 Adsorption energy of the O_2 molecule, $E_{ads}(O_2)$ (activation barrier for CO oxidation, E_{bar}(CO oxidation)) on Pd@TiO_2(110) and co-doped counterparts with V–C, V–N, Cr–C, Cr–N, and Cr–S co-dopant pairs.

tigate the kinetic processes of CO oxidation on the improved Pd@TiO_2(110) SACs. Typically, taking the p-type V–C and the n-type Cr–N co-doped cases as prototypical examples, we investigate the EMSI in optimizing CO oxidation rates by performing substantial simulations using the NEB method.[33]

First, three CO oxidation mechanisms proposed by recent theoretical studies[34,35] have been re-examined in the present work. Interestingly, we confirm that the CO oxidation prefers the Langmuir–Hinshelwood (L–H) process in both cases, *i.e.*, CO can also adsorb on the single Pd atom nearby the O_2 molecule and the co-adsorbed molecules undergo a bimolecular reaction through the formation of a CO_2 precursor, and then releasing the CO_2 molecule upon further activation. Note also that for both the pristine and the co-doped Pd@TiO_2(110) complexes, upon CO and O_2 co-adsorption, the Pd atom is located in almost the same position close to the surface V_O site, see also Fig. S1(B)† and Fig. 6. The detailed pathways and energetics for both cases are shown in Fig. 6. More specifically, as shown in Fig. 6(A), in the case of the p-typed V–C co-doped Pd@TiO_2(110) system (see structure (i)), we find that the first CO molecule easily adsorbs in the vicinity of the O_2 molecule on the Pd catalyst (structure (ii)) *via* the well-known back-donation charge transfer mechanism,[32,36] *i.e.*, donation of CO 5σ electrons to the Pd@TiO_2(110) substrate and back-donation from the Pd metal atom into the unoccupied 2π* orbital of CO. Here, we note that, as shown in Fig. 2, the upward-shifted HOMO and slightly downward shifted LUMO orbitals of the Pd atom promotes the back-donation process due to the enhanced EMSI. Consequently, the bond length of the adsorbed CO species is slightly enlarged to 1.154 Å from 1.143 Å of the gas phase, and correspondingly the C–O vibrational frequency is red shifted to 2037.56 cm^{-1} from 2120.64 cm^{-1}. Such a back-donation interaction effectively weakens the C–O bond strength and facilitates the formation of a bent CO_2 intermediate species when the CO molecule attacks the adsorbed O_2 species. Note that the modest activation of the CO as manifested by the red-shifted vibration frequency renders the Pd atom to be a good SAC candidate to avoid poisoning. An endothermic process with a low activation barrier of E_{bar} = 0.608 (see Fig. 6(A)-(iii)) for CO_2 formation and E_{bar} = 0.182 eV for CO_2 desorption are observed, respectively. Furthermore, when the first CO molecule is oxidized to release a CO_2, as presented in Fig. 6(A)-(iv), on the Pd atom there is still one O atom left which can be directly attached by the second incoming CO molecule during the formation of the second CO_2, *i.e.*, *via* the Eley–Rideal (E–R) mechanism (see Fig. 6(A)-(v)), with an activation barrier of only 0.211 eV. After this, a second round of O_2 activation and CO oxidation can be continued.

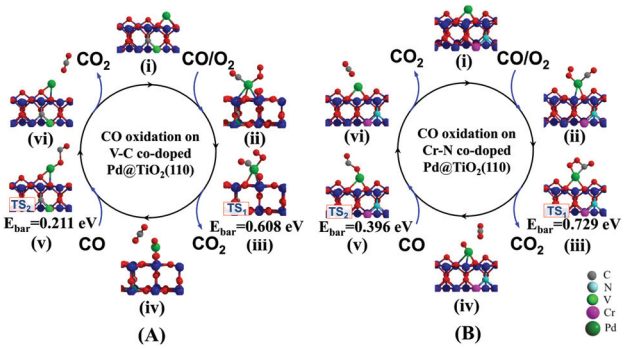

Fig. 6 Minimum energy paths for CO oxidation on Pd@TiO_2(110) co-doped with prototypical metal–nonmetal pairs. (A) p-Type V–C and (B) n-type Cr–N co-dopants.

For the case of n-type Cr–N co-doping, see Fig. 6(B)–(i), a slightly higher energy barrier of 0.729 eV (see structure (iii)) is detected for the first CO molecule oxidation *via* the L–H mechanism and 0.396 eV (see structure (v)) for the second CO molecule oxidation *via* the E–R process, respectively. Such similar rate-determining kinetic processes of the CO oxidation in these two cases can be ascribed to the comparable O_2 activations, as indicated by the negligible differences in the $E_{ads}(O_2)$ and enlarged O–O bond lengths, as well as the very close values of the red-shifted O–O vibrational frequencies. Here, we also emphasize that in the un-doped Pd@TiO_2(110), the large activation barrier for CO oxidation and the significantly small $E_{ads}(O_2)$ together dominated the low catalysis of the Pd SAC in the vicinity of the V_O. However, the calculated enlarged $E_{ads}(O_2)/E_{ads}(CO)$ of 0.808/0.705, 0.801/0.792, 0.794/0.606, and 0.732/0.443 eV on the p-type V–C, n-type Cr–N, compensated Cr–C, and compensated V–N co-doped Pd@TiO_2(110), along with the reduced E_{bar} values of 0.608, 0.729, 0.822 and 0.423 eV for CO oxidation render the Pd atom to be effective for CO oxidation on the same site as that in the un-doped TiO_2(110), demonstrating the crucial role of the EMSI in tuning the catalysis of the Pd atom. From Fig. 5, one can see that, the calculated values of the E_{bar} for the case of pristine Pd@TiO_2(110) and those of five co-doped cases establish an overall linear scale behavior as a function of the HOMO(Pd)–LUMO(O_2) gap, except for the case of the V–N co-doping, which slightly departs from the fitted linear trend due to the

relatively large energy gain upon the local geometric relaxation around the Pd single atom during the CO oxidation, see S5 of the ESI.† Importantly, we emphasize that an activation barrier of about 0.68 eV is calculated for CO oxidation on the Pd_2@TiO_2(110),[26] which was reported to possess good performance for CO oxidation in the experiment.[3] Therefore, the present results suggest that upon co-doping with low-cost metal–nonmetal pairs, the intrinsically inert noble Pd SAC is now expected to possess highly efficient catalysis for CO oxidation.

Conclusions

In conclusion, using the state-of-the-art first-principles calculations, we performed a comparative study on the electronic structures of a Pd single ad-atom over defective and metal–nonmetal co-doped TiO_2(110) substrates to establish the key role of the EMSI in optimizing the catalysis of SACs. *Via* the enhanced EMSI by co-doping, the intrinsically inert Pd atom on pristine TiO_2(110) can be tuned to serve as an effective electron charge reservoir sustained by the hybridized states of the co-dopant pairs to facilitate O_2 activation and CO oxidation. Interestingly, a close-linear correlation between the strength of the EMSI and the activation of the adsorbed O_2 molecule, as well as the energy barrier for CO oxidation, is observed in the cases of the Pd atoms deposited on both pristine TiO_2(110) and co-doped substrates with low-cost metal–nonmetal pairs. The present findings provide new insights into the understanding of the EMSI in heterogeneous catalysis and can open new avenues to design and fabricate highly efficient and cost-effective single-atom- and/or nanometer-sized catalysts.

Acknowledgements

We thank Professor Jun-Hyung Cho, Professor Yu Jia and Professor Zhenyu Zhang for helpful discussion. This work was supported by the NSFC (Grant No. 11074223, 11034006 and 11674289), and partly by the UK EPSRC (EP/L0183301/1) and US NSF (CMMI-1300223).

References

1 B. Qiao, A. Wang, X. Yang, L. F. Allard, Z. Jiang, Y. Cui, J. Liu, J. Li and T. Zhang, *Nat. Chem.*, 2011, **3**, 634–641.
2 M. Moses-DeBusk, M. Yoon, L. F. Allard, D. R. Mullins, Z. Wu, X. Yang, G. Veith, G. M. Stocks and C. K. Narula, *J. Am. Chem. Soc.*, 2013, **135**, 12634–12645.
3 W. E. Kaden, T. Wu, W. A. Kunkel and S. L. Anderson, *Science*, 2009, **326**, 826–829.
4 Q. Fu, H. Saltsburg and M. Flytzani-Stephanopoulos, *Science*, 2003, **301**, 935–938.
5 G. Vilé, D. Albani, M. Nachtegaal, Z. Chen, D. Dontsova, M. Antonietti, N. López and J. Pérez-Ramírez, *Angew. Chem., Int. Ed.*, 2015, **54**, 11265–11269.
6 N. Lopez, T. V. W. Janssens, B. S. Clausen, Y. Xu, M. Mavrikakis, T. Bligaard and J. K. Nørskov, *J. Catal.*, 2004, **223**, 232–235.
7 H. Zhang, T. Watanabe, M. Okumura, M. Haruta and N. Toshima, *Nat. Mater.*, 2012, **11**, 49–52.
8 L. Li, A. H. Larsen, N. A. Romero, V. A. Morozov, C. Glinsvad, F. Abild-Pedersen, J. Greeley, K. W. Jacobsen and J. K. Nørskov, *J. Phys. Chem. Lett.*, 2013, **4**, 222–226.
9 F. Li, Y. Li, X. C. Zeng and Z. Chen, *ACS Catal.*, 2015, **5**, 544–552.
10 X. Guo, G. Fang, G. Li, H. Ma, H. Fan, L. Yu, C. Ma, X. Wu, D. Deng, M. Wei, D. Tan, R. Si, S. Zhang, J. Li, L. Sun, Z. Tang, X. Pan and X. Bao, *Science*, 2014, **344**, 616–619.
11 S. Lee, C. Fan, T. Wu and S. L. Anderson, *J. Am. Chem. Soc.*, 2004, **126**, 5682–5683.
12 J. Zhang and A. N. Alexandrova, *J. Phys. Chem. Lett.*, 2013, **4**, 2250–2255.
13 S. J. Tauster, S. C. Fung and R. L. Garten, *J. Am. Chem. Soc.*, 1978, **100**, 170–175.
14 A. Bruix, J. A. Rodriguez, P. J. Ramírez, S. D. Senanayake, J. Evans, J. B. Park, D. Stacchiola, P. Liu, J. Hrbek and F. Illas, *J. Am. Chem. Soc.*, 2012, **134**, 8968–8974.
15 C. T. Campbell, *Nat. Chem.*, 2012, **4**, 597–598.
16 P. Hu, Z. Huang, Z. Amghouz, M. Makkee, F. Xu, F. Kapteijn, A. Dikhtiarenko, Y. Chen, X. Gu and X. Tang, *Angew. Chem., Int. Ed.*, 2014, **53**, 3418–3421.
17 O. Lopez-Acevedo, K. A. Kacprzak, J. Akola and H. Häkkinen, *Nat. Chem.*, 2010, **2**, 329–334.
18 M. Valden, X. Lai and D. W. Goodman, *Science*, 1998, **281**, 1647–1650.
19 S. Dahl, A. Logadottir, R. C. Egeberg, J. H. Larsen, I. Chorkendorff, E. Törnqvist and J. K. Nørskov, *Phys. Rev. Lett.*, 1999, **83**, 1814–1817.
20 J. K. Norskov, T. Bligaard, B. Hvolbaek, F. Abild-Pedersen, I. Chorkendorff and C. H. Christensen, *Chem. Soc. Rev.*, 2008, **37**, 2163–2171.
21 P. Hohenberg and W. Kohn, *Phys. Rev. B*, 1964, **136**, B864.
22 G. Kresse and J. Hafner, *Phys. Rev. B: Condens. Matter*, 1994, **49**, 14251.
23 P. E. Blochl, *Phys. Rev. B: Condens. Matter*, 1994, **50**, 17953.
24 J. P. Perdew, K. Burke and M. Ernzerhof, *Phys. Rev. Lett.*, 1996, **77**, 3865.
25 C. Xu, X. Lai, G. W. Zajac and D. W. Goodman, *Phys. Rev. B: Condens. Matter*, 1997, **56**, 13464–13482.
26 S. Li, X. Zhao, J. Shi, Y. Jia, Z. Guo, J.-H. Cho, Y. Gao and Z. Zhang, *Phys. Chem. Chem. Phys.*, 2016, **18**, 24872.
27 S. B. Zhang, *J. Phys.: Condens. Matter*, 2002, **14**, R881.
28 W. Zhu, X. Qiu, V. Iancu, X.-Q. Chen, H. Pan, W. Wang, N. M. Dimitrijevic, T. Rajh, H. M. Meyer, M. P. Paranthaman, G. M. Stocks, H. H. Weitering, B. Gu, G. Eres and Z. Zhang, *Phys. Rev. Lett.*, 2009, **103**, 226401.
29 H. Häkkinen, S. Abbet, A. Sanchez, U. Heiz and U. Landman, *Angew. Chem., Int. Ed.*, 2003, **42**, 1297–1300.

30 I. N. Remediakis, N. Lopez and J. K. Nørskov, *Angew. Chem., Int. Ed.*, 2005, **44**, 1824–1826.
31 B. Hammer, Y. Morikawa and J. K. Norskov, *Phys. Rev. Lett.*, 1996, **76**, 2141–2144.
32 L. P. A. Nilsson and J. K. Nørskov, *Chemical Bonding at Surfaces and Interfaces*, Elsevier, Amsterdam, 2008.
33 G. Henkelman, B. P. Uberuaga and H. Jónsson, *J. Chem. Phys.*, 2000, **113**, 9901–9904.
34 H. Y. Kim, H. M. Lee and G. Henkelman, *J. Am. Chem. Soc.*, 2012, **134**, 1560–1570.
35 C. Zhang, A. Michaelides and S. J. Jenkins, *Phys. Chem. Chem. Phys.*, 2011, **13**, 22–33.
36 R. Hoffmann, *Rev. Mod. Phys.*, 1988, **60**, 601–628.